Int J Adv Manuf Technol (2016) 87:3211–3224
DOI 10.1007/s00170-016-8726-x

ORIGINAL ARTICLE

# A model for grinding forces prediction in ultrasonic vibration assisted grinding of SiCp/Al composites

**Ming Zhou**[1] · **Wei Zheng**[1]

Received: 11 January 2016 / Accepted: 4 April 2016 / Published online: 12 April 2016


**Abstract** Ultrasonic vibration assisted grinding is an advanced method for machining difficult-to-process materials such as SiCp/Al composites. This paper presents a mechanics model for predicting grinding forces in ultrasonic vibration assisted grinding of SiCp/Al composites. It consists of side grinding force model and end grinding force model. In side grinding force model, the major components are the normal force and tangential force in which the analytical expressions for the chip formation force based on Rayleigh's probability density function, the frictional force, and the particle fracture force based on Griffith theory are established, respectively. In contrast, the axial force developed based on the indentation theory is the major component in end grinding force model. The coefficients in the proposed grinding force model were obtained through two groups of orthogonal experiments. Based on the mechanics prediction model, the relationship between grinding forces and process variables were predicted. At last, two groups of single factor experiments were conducted to verify the proposed grinding force model and experimental results were found to agree well with predicted results.

**Keywords** Ultrasonic vibration assisted grinding · SiCp/Al composites · Grinding force · Prediction model

✉ Wei Zheng
zhengwhit@gmail.com

Ming Zhou
zhouming@hit.edu.cn

[1] School of Mechanical and Electrical Engineering, Harbin Institute of Technology, No. 92, West Da-Zhi Street, Harbin, Heilongjiang 150001, People's Republic of China

## 1 Introduction

Superior properties such as high specific strength and specific stiffness make SiCp/Al composites highly competitive against conventional materials and are widely used in aerospace, automobile, and other fields. However, the addition of SiC particles makes SiCp/Al composites hard to be manufactured because of its extreme abrasive properties. This has limited the practical application of SiCp/Al composites. Therefore, it is necessary to develop a nontraditional machining process to meet the demand of SiCp/Al composite machining. Ultrasonic vibration assisted grinding is a combination of two ordinary material remove processes, i.e., grinding and ultrasonic machining, during which ultrasonic vibration is applied to the grinding tool. Compared with other traditional machining methods, this machining method has many advantages, such as lower grinding force, higher surface quality, higher machining efficiency, and longer tool life [1–5].

The machining of SiCp/Al composites has been extensively studied experimentally and numerically to assess tool wear, tool life, surface roughness, and subsurface damage. There are a few studies focused on the prediction model of cutting forces in cutting or conventional grinding of metal matrix composites (MMCs) [6–12]. Kishawy et al. [6] presented an energy-based analytical force model in orthogonal cutting of SiCp/Al composites to predict cutting forces. In this model, the energy for interfacial debonding is quantified. Pramanik et al. [7] developed a mechanics model for cutting force prediction when a machining aluminum-based $SiC/Al_2O_3$ particle reinforced MMCs. In this model, cutting force is considered to consist of components due to chip formation, ploughing, particle fracture, and displacement. Davim [8] presented a preliminary experimental study based on Merchant theory, in which the chip compression ratio, shear angle, shear strain, shear strain rate, normal stress, and shear stress were evaluated. Dabade

et al. [9] developed a cutting force prediction model in turning SiCp/Al composites, in which the frictional characteristics of chip–tool and work–tool interfaces were considered. Sikder et al. [10] presented an analytical prediction force model in turning SiCp/Al composites. In this model, the frictional force along the chip–tool interface was modeled. Du et al. [11] developed an analytical cutting force model for conventional grinding SiCp/Al composites based on the energy theory of particle fracture and Griffith theory of fracture. But, in this model, only side grinding force was modeled. Ghandehariun et al. [12] presented a novel analytical force model in machining MMCs which was based on the calculation of power consumption in different parts of the cutting system. The plastic deformations, different types of friction at various interfaces, and debonding and fracture of reinforcements were considered in the model.

It is noted that, at present, no publications are available on grinding force model for ultrasonic vibration assisted grinding SiCp/Al composites. Therefore, this paper develops a numerical model for grinding force prediction in ultrasonic vibration assisted grinding of SiCp/Al composites to help optimize process variables.

The paper is organized into five sections. Following this introduction section, Sect. 2 describes the grinding force model development step by step. In Sect. 3, experimental setup is introduced. The coefficients in the proposed model is determined through two groups of orthogonal experiments, predicted influences of process variables on grinding forces are discussed, and two groups of single factor experiments were conducted to verify the proposed grinding force model in Sect. 4. Conclusions are contained in Sect. 5.

## 2 Development of grinding force model

Ultrasonic vibration assisted grinding contains two different machining modes: side grinding and end grinding, as shown in Fig. 1. Then, grinding force in ultrasonic vibration assisted grinding of SiCp/Al composites can be divided into two parts: the side grinding force and the end grinding force. In side grinding process, the normal force and the tangential force are the major components of the side grinding force. In contrast, in end grinding process, the major component of the end grinding force is the axial force. Side grinding force model and end grinding force model will be developed respectively in Sects. 2.2 and 2.3.

The development of the grinding force model is based on the following several major assumptions and simplifications:

1. The diamond abrasive grains are assumed to be rigid cones with the same generatrix $s$ and semi-angle $\theta = 60°$, as shown in Fig. 2.
2. All diamond abrasive grains uniformly distribute in the abrasive portion of the grinding tool, and all of them take part in cutting process during each ultrasonic vibration cycle.
3. During the development of the grinding force model, only stable machining process is taken into account; i.e., the cutting in and out processes of the grinding tool are neglected.
4. Ultrasonic vibration amplitude $A$ and frequency $f$ in the machining process are in a stable condition; i.e., both of them keep unchanged during machining.

### 2.1 Kinematic analysis of abrasive grains in ultrasonic vibration assisted grinding

Since the abrasive grains, both on side and end surfaces of the grinding tool, vibrate at an amplitude $A$ and a frequency $f$ while feeding with a feedrate $v_f$ and an angular speed $\omega$, the motion and speed of a single abrasive grain in the x, y, and z directions can be expressed as follows:

$$s_g(t) = \begin{pmatrix} x_g(t) \\ y_g(t) \\ z_g(t) \end{pmatrix} = \begin{pmatrix} v_f t + R_o \sin(\omega t) \\ R_o \cos(\omega t) \\ A \sin(2\pi f t) \end{pmatrix} \tag{1}$$

$$v_g(t) = s_g'(t) = \begin{pmatrix} x_g'(t) \\ y_g'(t) \\ z_g'(t) \end{pmatrix} = \begin{pmatrix} v_f + \omega R_o \cos(\omega t) \\ -\omega R_o \sin(\omega t) \\ 2\pi f A \cos(2\pi f t) \end{pmatrix} \tag{2}$$

where $R_i$ and $R_o$ are the inner and outer radii of the grinding tool, respectively.

The motion trajectories of grains on side and end surfaces of the grinding tool are shown in Fig. 3.

### 2.2 Development of side grinding force model

Side grinding force can be subdivided into chip formation force, ploughing force, friction force, and fracture force of silicon carbide particles (SiCp) [6, 7, 11, 13, 14]. The ploughing force is neglected in this numerical model as it is much lesser than the other forces [15].

Then, the total side grinding force $F_{SG}$, normal force $F_n$, and tangential force $F_t$ can be expressed respectively as Eqs. (3)~(4):

$$F_{SG} = F_{chip} + F_{friction} + F_{fracture} = F_n + F_t \tag{3}$$

$$\begin{aligned} F_n &= F_{nc} + F_{nr} + F_{na} \\ F_t &= F_{tc} + F_{tr} + F_{ta} \end{aligned} \tag{4}$$

where $F_{nc}$ is normal component of chip formation force, $F_{nr}$ is normal component of frictional force, $F_{na}$ is normal component of fracture force, $F_{tc}$ is tangential component of chip formation force, $F_{tr}$ is tangential component of frictional force, and $F_{ta}$ is tangential component of fracture force.

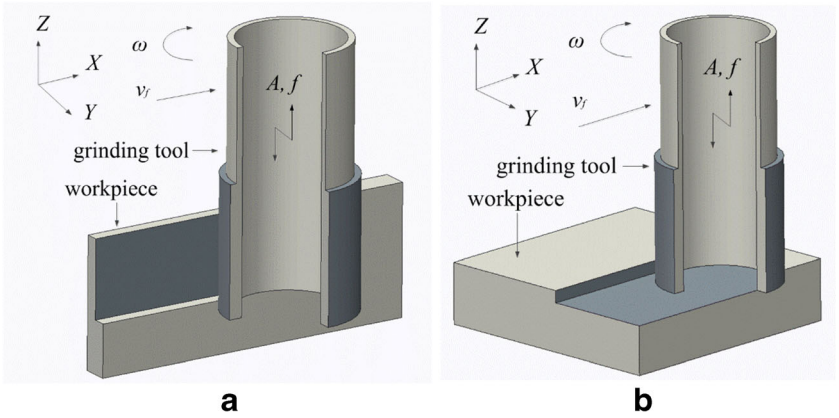


**Fig. 1** Schematic diagram of two different machining modes: side grinding (**a**) and end grinding (**b**)

*2.2.1 Dynamic motion of a single grain in side grinding*

As shown in Fig. 4, in side grinding process, an abrasive grain cuts in at point B and out at point A, so the cutting depth $a_p$ (mm) can be expressed as

$$a_p = R_o(1-cos\omega\Delta T) \tag{5}$$

where $\Delta T$ is the effective time between cutting in and out of the workpiece.

Considering $\omega\Delta T$ is close to 0, it can be simplified as

$$\cos\omega\Delta T = 1-\frac{(\omega\Delta T)^2}{2} \tag{6}$$

where $\omega = \frac{v_c}{R_o}$.

Substituting Eq. (6) into Eq. (5), the effective cutting time can be obtained

$$\Delta T = \frac{\sqrt{2a_pR_o}}{v_c} \tag{7}$$

where $v_c$ is the linear speed of the grinding tool.

In ultrasonic vibration assisted side grinding process, the geometric contact length $l_a$ and dynamic contact length $l_b$ can be calculated respectively:

$$l_a = \widehat{AB} = v_c\Delta T = \sqrt{2a_pR_o} \tag{8}$$

$$\begin{aligned} l_b &= \int_0^{\Delta T} |v_{gt}|dt \\ &= \int_0^{\Delta T} \sqrt{(v_f+\omega R_o\cos(\omega t))^2 + (-\omega R_o\sin(\omega t))^2 + (2\pi fA\cos(2\pi ft))^2}dt \end{aligned} \tag{9}$$

Setting $X=(v_f+v_c)t$, $Y=A\sin(2\pi ft)$, then $l_b$ can also be expressed as

$$\begin{aligned} l_b &= \int_0^l \sqrt{1+\left(dY/dX\right)^2}dX \\ &= \int_0^l \sqrt{1+\left(\frac{2\pi fA}{v_f+v_c}\cos\left(\frac{2\pi f}{v_f+v_c}X\right)\right)^2}dX \end{aligned} \tag{10}$$

where $l=\int_0^{\Delta T}(v_f+v_c)dt \approx l_a$.

*2.2.2 Chip formation force*

The cutting process of a single grain of the tool is similar to the process of a single cutting tool in turning [16]. As shown in

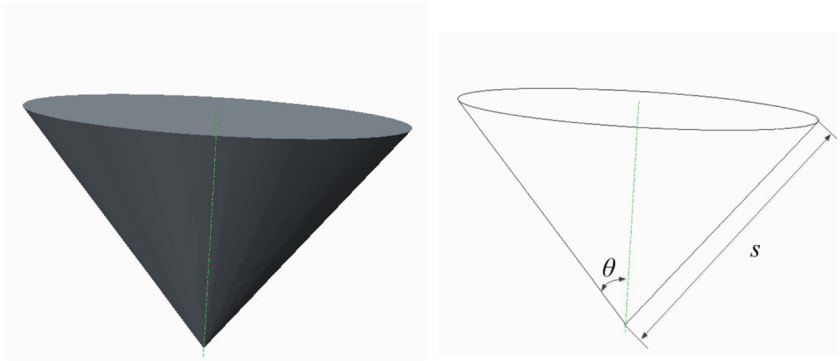


**Fig. 2** Schematic diagram of an abrasive grain

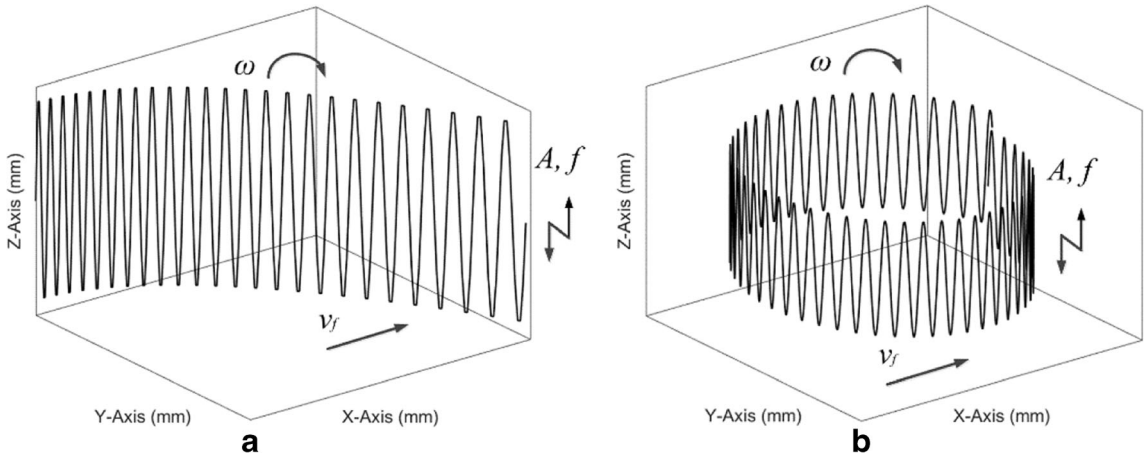


**Fig. 3** Motion trajectories of grains on side (**a**) and end (**b**) surface of the grinding tool

Fig. 5, in the X–X cross-sectional area, grinding force of a single grain can be expressed as

$$dF_x = F_p dA_g \cos\theta\cos\psi \tag{11}$$

where $F_p$ is the grinding force per unit area, $\psi$ is the angle between grinding force direction, and $X$ is the direction.

The center line of the grains points to the center of the grinding tool along the radius direction, then the contact area between a single grain and the workpiece can be expressed as

$$dA_g = \frac{1}{2}s^2 \sin\theta d\psi \tag{12}$$

Substituting Eq. (12) into Eq. (11),

$$dF_x = \frac{1}{2}s^2 F_p \sin\theta\cos\theta\cos\psi d\psi \tag{13}$$

Then the normal and tangential chip formation force of a single grain can be expressed as

$$\begin{aligned} dF_{tgc} &= dF_x \cos\theta\cos\psi = \frac{1}{2}s^2 F_p \sin\theta\cos^2\theta\cos^2\psi d\psi \\ dF_{ngc} &= dF_x \sin\theta = \frac{1}{2}s^2 F_p \sin^2\theta\cos\theta\cos\psi d\psi \end{aligned} \tag{14}$$

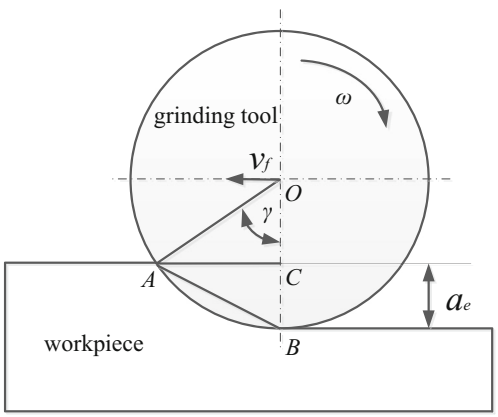


**Fig. 4** Schematic diagram of side grinding process

Under the influence of the ultrasonic vibration, as shown in Fig. 6, there exists an angle $\varphi$ between grain motion direction and tangential direction, which can be expressed as

$$\varphi = \arctan\frac{A\omega\cos\omega t}{v_c} \tag{15}$$

Then the normal and tangential chip formation force of a single grain can be determined as

$$\begin{aligned} F_{ngc} &= \int_{-\pi/2+\varphi}^{\pi/2+\varphi} dF_{ngc} = F_p \overline{h}^2 \sin\theta\tan\theta\cos\varphi \\ F_{tgc} &= \int_{-\pi/2+\varphi}^{\pi/2+\varphi} dF_{tgc} = \frac{\pi}{4}F_p \overline{h}^2 \sin\theta \end{aligned} \tag{16}$$

where $\overline{h}$ is the average cutting depth, i.e., undeformed chip thickness.

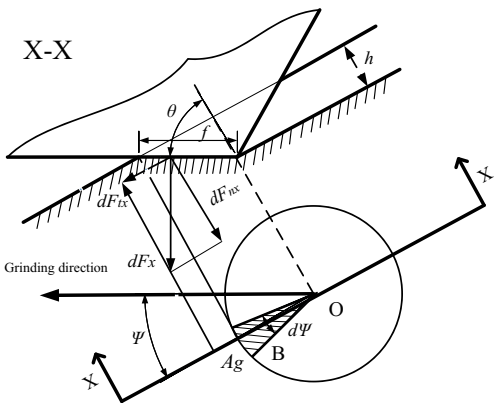


**Fig. 5** Schematic diagram of force model of a single grain in side grinding

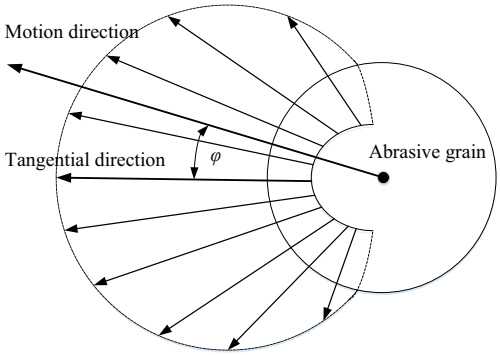


**Fig. 6** Schematic diagram of $\varphi$ between motion direction and tangential direction

Several research results [17, 18] show that the undeformed chip thickness can be described by Rayleigh's probability density function, which is given by

$$f(h) = \begin{cases} \left(h/m^2\right)e^{-\left(h^2/2m^2\right)} & h \geq 0 \\ 0 & h < 0 \end{cases} \tag{17}$$

where $m$ is a parameter that completely defines the probability density function, and it depends upon the cutting conditions, microstructure of grinding tool, and the properties of workpiece material. The expected value and standard deviation of the above function can be expressed as

$$E(h) = \sqrt{\frac{\pi}{2}}m \tag{18}$$

$$\sigma(h) = \sqrt{\frac{4-\pi}{2}}\,m \tag{19}$$

The expected value of undeformed chip thickness area $A_{ct}$ can be expressed as

$$E(A_{ct}) = E\left(h^2\right)tan\theta \tag{20}$$

Then the expected value of the total material removal volumes by all active grains can be expressed as

$$V_g = N_s E(A_{ct}) l_b \tag{21}$$

where $N_s$ is the number of active grains in the contact area which can be obtained according to the definition of abrasive concentration. Since abrasive particle is simplified as a regular cone, the number of active abrasive grains can be obtained by the following equation:

$$N_s = \left[\frac{0.88 \times 10^{-3}}{\frac{1}{3}\pi(ssin\theta)^2 s\cos\theta\rho}\frac{C_a}{100}\right]^{2/3} bl_a = k\frac{{C_a}^{2/3}}{s^2}bl_a \tag{22}$$

where $k$ is a constant, $\rho$ is the density of the abrasive grain material, $\rho$=3.52e-3 g/mm$^3$ for diamond, $C_a$ is the abrasive concentration of the tool, and $b$ is the cutting width.

In addition, the total material removal volumes can also be calculated as

$$V_g = a_p b v_f \Delta T \tag{23}$$

Substituting Eqs. (20) and (21) into Eq. (23), the expected value of $h^2$ can be obtained:

$$E\left(h^2\right) = \frac{a_p v_f \Delta T}{k\frac{{C_a}^{2/3}}{s^2} l_a l_b \tan\theta} \tag{24}$$

$E(h^2)$ can also be calculated as

$$E\left(h^2\right) = \int_0^\infty h^2 f(h) dh \tag{25}$$

Substituting Eqs. (17), (24), and (25) into Eq. (18), the undeformed chip thickness can be obtained:

$$\overline{h} = \sqrt{\frac{\pi a_p v_f}{4k\frac{{C_a}^{2/3}}{s^2} l_b v_c \tan\theta}} \tag{26}$$

Substituting Eq. (26) into Eq. (16), setting $C_1 = \frac{1}{8}F_p\sin\theta$ and $C_2 = \frac{\pi}{32}F_p\cos\theta$, the normal and tangential chip formation force can be determined by multiplying $N_a$

$$\begin{aligned} F_{nc} &= C_1\frac{l_a\ v_f}{l_b n R_o} ba_p\cos\varphi \\ F_{tc} &= C_2\frac{l_a\ v_f}{l_b n R_o} ba_p \end{aligned} \tag{27}$$

where $C_1$ and $C_2$ are experimental coefficients which can be determined through experiments in Sect. 4.1.1, and $n$ is the spindle speed.

### 2.2.3 Frictional force

The wear of the grains in the flat area of the grinding wheel results in the frictional force [11, 16]. Assuming that SiC particles are not fractured in the rubbing process, the frictional behavior in grinding SiCp/Al composites is similar to that of metal materials. Hence, the normal and tangential frictional force can be expressed as follows:

$$\begin{aligned} F_{nr} &= N_s \tau p \\ F_{tr} &= \mu_g N_s \tau p \end{aligned} \tag{28}$$

where $\tau$ is the real contact area between the grinding tool and workpiece. $p$ is the average contact pressure between the grinding tool and workpiece. $\mu_g$ is the coefficient of friction.

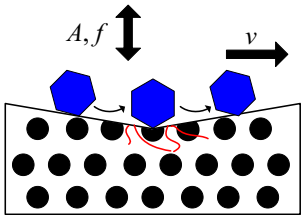


**Fig. 7** Material removal mode: the interaction of impacting and erosion

In the geometric dynamics analysis of grinding grains, using parabola function to approximate the cutting path, the deviation between grinding wheel radius and the radius of curvature of the cutting path can be expressed as

$$\Delta = \frac{2v_f}{v_c R_o} \tag{29}$$

The average contact pressure between workpiece and abrasive grain wear plane approximately linearly increases with the deviation of curvature radius increases and can be expressed as

$$p = p_0 \Delta = \frac{2p_0 v_f}{v_c R_o} \tag{30}$$

where $p_0$ is the proportionality constant.

The average contact pressure between workpiece and abrasive grains wear plane varies with grinding parameters. Therefore, there is likely to exist elastic contact, elastic–plastic contact, or plastic contact. Therefore, the frictional coefficient also varies with the average contact pressure. According to the frictional binomial theorem, the frictional coefficient can be expressed as

$$\mu_g = \frac{\alpha}{p} + \beta \tag{31}$$

where $\alpha$ and $\beta$ are coefficients which are determined by physical and mechanical properties of contact interface.

Substituting Eqs. (30)~(31) into Eq. (28), setting $C_3 = \frac{\sqrt{2}}{\pi}\tau k p_0$, $C_4 = \sqrt{2}\tau k$, and $C_5 = \frac{\sqrt{2}}{\pi}\tau\beta k p_0$, the total normal and tangential frictional forces can be expressed as

$$\begin{aligned} F_{nr} &= C_3 \frac{v_f}{nR_o} \frac{{C_a}^{2/3}}{s^2} b\sqrt{\frac{a_p}{R_o}} \\ F_{tr} &= C_4 \frac{{C_a}^{2/3}}{s^2} b\sqrt{a_p R_o} + C_5 \frac{v_f}{nR_o} \frac{{C_a}^{2/3}}{s^2} b\sqrt{\frac{a_p}{R_o}} \end{aligned} \tag{32}$$

where $C_3$~$C_5$ are experimental coefficients which can be determined through experiments in Sect. 4.1.1.

### 2.2.4 Fracture force

Cracking damage of the ceramic particle is assumed to be controlled by the stress in the particle and the statistical behavior of the strength of the particle [6, 10]. So based on Griffith theory, the change in the potential energy of the composite due to the debonding damage is a function of the volume fraction of the SiC particles and the material properties, as shown in Eq. (33):

$$G = \frac{dU}{dS} = \frac{K^2(1-\nu^2)}{E} \tag{33}$$

$$K^2 = \pi\sigma^2 l \tag{34}$$

$$dS = wdl \tag{35}$$

$$\sigma = \frac{K_{IC}}{\sqrt{d}} \tag{36}$$

where $U$ is the strain energy, $S$ is the change in interface crack area, $K$ is stress intensity, $\nu$ is the Poisson's ratio, $E$ is the elastic modulus of the SiC particle, $\sigma$ is the fracture stress of the SiC particle, $l$ is the interface crack length, $w$ is the initial interface crack width, $K_{IC}$ is the fracture toughness of the SiC particle, and $d$ is the size of the SiC particle.

The initial interface crack length $l_i$ and the initial interface crack width $w$ are assumed to be 1 μm; the final crack length $l_f$

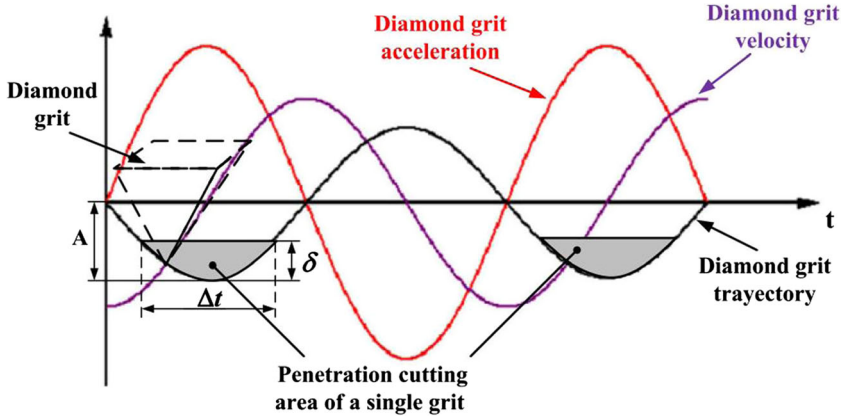


**Fig. 8** Schematic diagram of the effective cutting time Δt in end grinding [21]

**Table 1** Properties of the grinding tool used in experiments

| Abrasive size $s$ (μm) | Abrasive concentration Ca | Outer radius $R_o$ (mm) | Inner radius $R_i$ (mm) |
|---|---|---|---|
| 75 | 100 | 30 | 20 |

is assumed to be equal to the circumference of the SiC particle [6, 10]. Hence, substituting Eqs. (34), (35), and (36) into Eq. (33), the strain energy consumed for fracture can be determined as follows:

$$U = \int_{l_i}^{l_f} \frac{\pi w {K_{IC}}^2 (1-\nu^2)}{Ed} ldl \tag{37}$$

The research results of [11, 19] indicate that the fracture fraction of SiC particles is equal to the volume fraction; the number of fractured and debonding SiC particles per unit volume can be expressed as follows:

$$n_f = \frac{1}{\frac{4}{3}\pi\left(\frac{d}{2}\right)^3} v_d^2 \tag{38}$$

where $v_d$ is the volume fraction of SiC particles.

According to the energy conservation law, the relationship between the fracture force and the strain energy consumed for fracture can be expressed as

$$F_{fracture} = n_f U b a_p \tag{39}$$

Substituting Eqs. (7), (23), (37), and (38) into Eq. (39), and setting $C_6 = n_f U \cos\theta$ and $C_7 = n_f U \sin\theta$, the total normal and tangential fracture forces can therefore be obtained:

$$\begin{aligned} F_{na} &= C_6 b a_p \\ F_{ta} &= C_7 b a_p \end{aligned} \tag{40}$$

where $C_6$ and $C_7$ are experimental coefficients of the normal and tangential fracture forces, respectively, which can be determined through experiments in Sect. 4.1.1.

**Table 2** Experimental parameters for obtaining coefficients $C_1$~$C_7$ in side grinding force model

| Levels | Spindle speed $n$ (rpm) | Feedrate $v_f$ (mm/min) | Cutting depth $a_p$ (mm) | Cutting width $b$ (mm) |
|---|---|---|---|---|
| 1 | 8000 | 100 | 0.05 | 1 |
| 2 | 10,000 | 150 | 0.1 | 3 |
| 3 | 12,000 | 200 | 0.15 | 5 |

**Table 3** Coefficients $C_1$~$C_7$ in side grinding force model

| $C_1$ | $C_2$ | $C_3$ | $C_4$ | $C_5$ | $C_6$ | $C_7$ |
|---|---|---|---|---|---|---|
| 4519.5 | 1895.3763 | 331,949 | 150.514 | 45,835.2 | 9.1 | 19.1 |

### 2.2.5 The side grinding force model

Substituting Eqs. (4), (27), (32), and (40) into Eq. (3), the side grinding force model can be determined as follows:

$$F_{SG} = \begin{cases} C_1 \frac{l_a}{l_b} \frac{v_f}{n R_o} b a_p \cos\varphi + C_3 \frac{v_f}{n R_o} \frac{{C_a}^{2/3}}{s^2} b \sqrt{\frac{a_p}{R_o}} + C_6 b a_p \\ C_2 \frac{l_a}{l_b} \frac{v_f}{n R_o} b a_p + C_4 \frac{{C_a}^{2/3}}{s^2} b \sqrt{a_p R_o} + C_5 \frac{{C_a}^{2/3}}{s^2} \frac{v_f}{n R_o} b \sqrt{\frac{a_p}{R_o}} + C_7 b a_p \end{cases} \tag{41}$$

## 2.3 Development of end grinding force model

When the grinding tool feeds into SiCp/Al composites, an abrasive grain on the end face of the grinding tool is not in continuous contact with the workpiece due to ultrasonic vibration. So in the end grinding process, there are two different material removal modes between the abrasive grains and SiCp/Al composites—impact and erosion—as shown in Fig. 7. Due to the influence of the high vibration frequency, the impact mode is the major component in the end grinding process.

So the total end grinding force $F_{EG}$ is mainly composed of the impact force $F_{impact}$ and can be expressed as follows:

$$F_{EG} = F_{impact} \tag{42}$$

### 2.3.1 Dynamic motion of a single grain in end grinding

In each ultrasonic vibration cycle of the grinding tool, the abrasive grain makes contact with the workpiece only at a certain period of time, i.e., effective cutting time $\Delta t$, as shown in Fig. 8. It will take an abrasive grain on the end face of the

**Table 4** Experimental parameters for obtaining coefficients $C_8$~$C_{11}$ in end grinding force model

| Levels | Spindle speed $n$ (rpm) | Feedrate $v_f$ (mm/min) | Cutting depth $a_p$ (mm) |
|---|---|---|---|
| 1 | 9000 | 100 | 0.04 |
| 2 | 12,000 | 150 | 0.06 |
| 3 | 15,000 | 200 | 0.08 |
| 4 | 18,000 | 250 | 0.1 |

**Table 5** Coefficients $C_8$~$C_{11}$ in end grinding force model

| $C_8$ | $C_9$ | $C_{10}$ | $C_{11}$ |
|---|---|---|---|
| 55,436.8603 | −0.738 | 0.218 | 0.165 |

grinding tool $\Delta t/2$ to move from $z=A-\delta$ to $z=A$. $\Delta t$ can be calculated by the following equation [20]:

$$\Delta t = \frac{\delta}{2Af} \propto \frac{\delta}{Af} \tag{43}$$

### 2.3.2 Impact force

Several research results [22–24] indicate that SiCp/Al composites show different micro-properties with different indention experiment conditions such as loading point, loading rate, loading value, and indention depth. So, in this section, SiCp/Al composites are simplified as an equivalent homogenous metal material with the same properties, hence the maximum impact force induced by the maximum penetration can be expressed by the following equation:

$$F_m = \frac{1}{2}\sigma_y \pi(\delta \sin\theta)^2 N_m \propto \delta^2 N_m \tag{44}$$

where $\sigma_y$ is the compressive strength of the material, $\delta$ is the maximum penetration depth of an abrasive grain on the end face of the grinding tool, and $N_m$ is the number of abrasive particles on the end face of the grinding tool which can be obtained by the following equation

$$N_m = k\frac{C_a{}^{2/3}}{s^2}\frac{\pi\left(R_o^2 - R_i^2\right)}{2} \propto \frac{C_a{}^{2/3}}{s^2} \tag{45}$$

Then, the average impact force in a vibration cycle can be calculated as follows:

$$F_{impact} = F_m f \Delta t \tag{46}$$

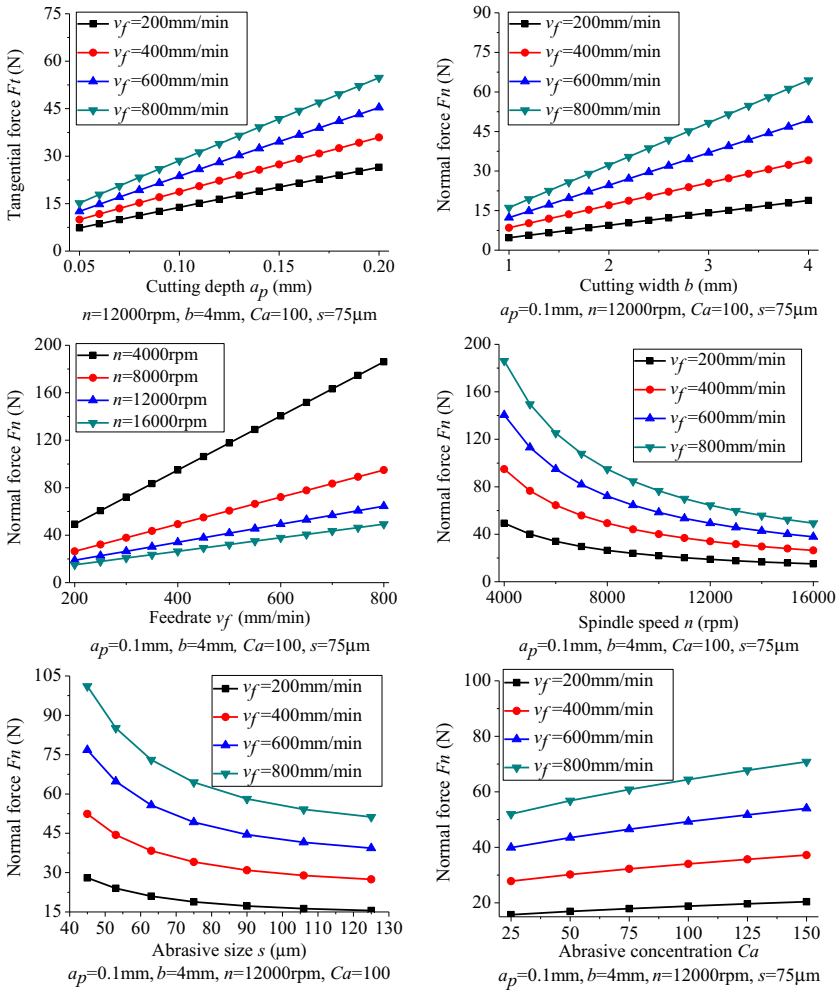


**Fig. 9** Predicted relationship between the normal force and process variables

Substituting Eqs. (43), (44), and (45) into Eq. (46), the relationship between the impact force and the maximum penetration depth can be obtained:

$$F_{impact} \propto \frac{\delta^3 {C_a}^{2/3}}{As^2} \tag{47}$$

### 2.3.3 Actual volume removed in a vibration cycle

Compared with the spindle speed, the feed speed is much lesser; this paper assumes that the influence of feed motion can be neglected in the calculation of effective cutting distance that an abrasive grain scratches during effective cutting time. So the effective cutting distance can be calculated by the following equation:

$$l_s = \frac{2\pi nR}{60}\Delta t \propto n\frac{\delta}{Af} \tag{48}$$

where $R$ is the average radius of the tool and can be expressed as

$$R = \frac{1}{2}(R_i + R_o) \tag{49}$$

At the same time, the abrasive grain scratches SiCp/Al composites when the penetration increases from 0 to $\delta$ and decreases to 0. So the volume of material removed by one abrasive grain in a vibration cycle can be described as a pyrometric cone and can be obtained from the following equation:

$$V_e = \frac{1}{3} l_s \delta^2 \tan\theta \propto n\frac{\delta^3}{Af} \tag{50}$$

Considering the interrelations among abrasive grains, the feed motion of the grinding tool, and the fracture of SiC particles, the actual volume of material removed in a vibration cycle is different from the theoretical volume. Assuming that the actual volume is in terms of the theoretical volume and

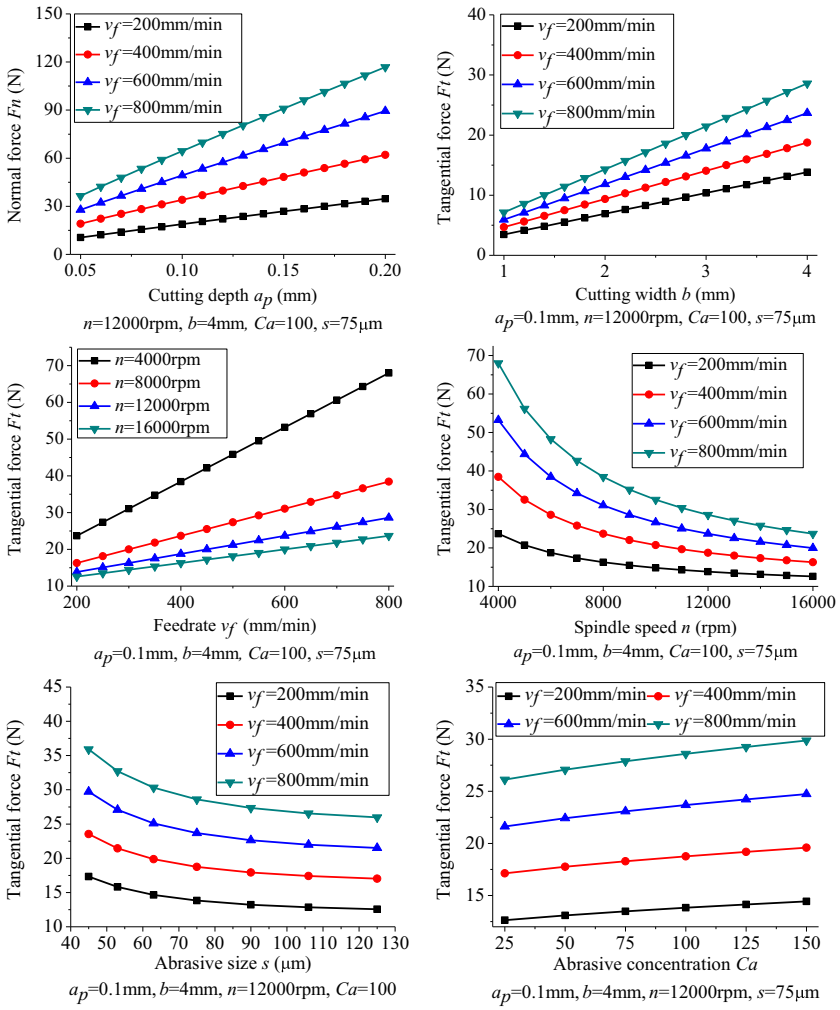


**Fig. 10** Predicted relationship between the tangential force and process variables

cutting parameters, then the actual volume in a vibration cycle can be expressed as

$$V_m = c_8 n^{c_9} a_p^{c_{10}} v_f^{c_{11}} N_m V_e \propto n^{c_9+1} a_p^{c_{10}} v_f^{c_{11}} \frac{C_a^{2/3}}{s^2} \frac{\delta^3}{Af} \tag{51}$$

In addition, actual volume of material removed in a vibration cycle can also be expressed as follows:

$$V_m = Abv_f \Delta t \propto v_f \frac{\delta}{f} \tag{52}$$

### 2.3.4 The end grinding force model

Substituting Eqs. (48), (49), (50), and (52) into Eq. (51), the relationship between process parameters and the maximum penetration depth can be obtained:

$$\delta^2 \propto \frac{As^2}{C_a^{2/3} n^{c_9+1} a_p^{c_{10}} v_f^{c_{11}-1}} \tag{53}$$

Then the relationship between the impact force and process parameters can be obtained by solving Eqs. (47) and (53):

$$F_{impact} \propto \frac{A^{1/2} s}{C_a^{1/3} n^{3(c_9+1)/2} a_p^{3c_{10}/2} v_f^{3(c_{11}-1)/2}} \tag{54}$$

Setting $C_8$ as a constant coefficient, $C_9 = -3(c_9+1)/2$, $C_{10} = -3c_{10}/2$, and $C_{11} = -3(c_{11}-1)/2$, the end grinding force model can be determined as follows:

$$F_{EG} = \frac{C_8 A^{1/2} s}{C_a^{1/3}} n^{C_9} a_p^{C_{10}} v_f^{C_{11}} \tag{55}$$

where $C_8$~$C_{11}$ are experimental coefficients which can be determined through experiments in Sect. 4.1.2.

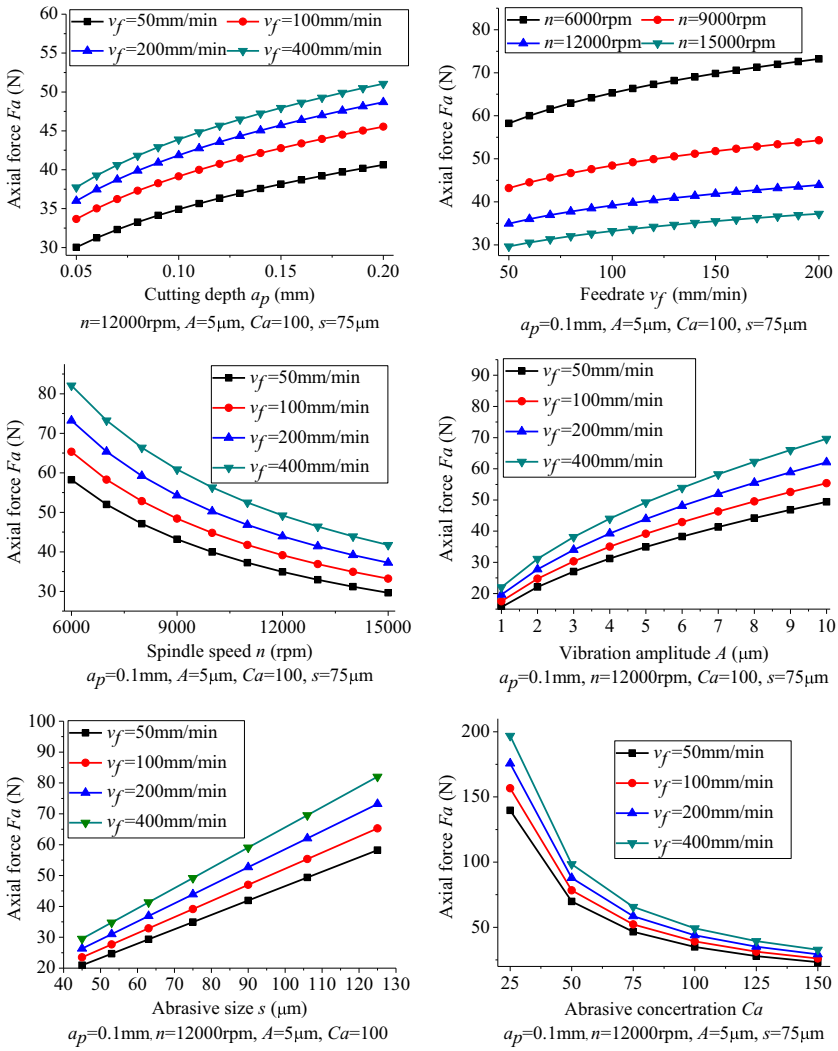


**Fig. 11** Predicted relationship between the axial force and process variables

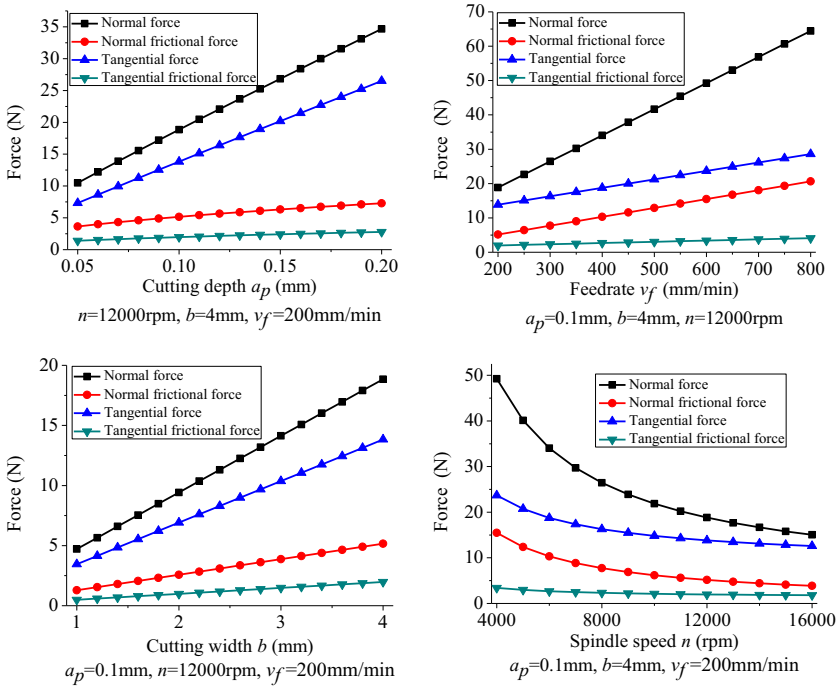


**Fig. 12** Comparisons of the frictional force, normal force, and tangential force

## 3 Experimental setup

Ultrasonic vibration assisted grinding experiments were conducted on an ultrasonic vibration machine center (DMG Ultrasonic70-5 linear), which consisted a numerical control system, an ultrasonic spindle system, a data acquisition system, and a coolant system. The maximum spindle speed was 18,000 rpm. The frequency and amplitude supplied to the tool in the z direction were about 30 kHz and 5 μm, respectively. The grinding tool with metal-bonded diamond abrasives was provided by SCHOTT Company, and its properties were listed in Table 1. The grinding forces were measured by a three-component dynamometer type 9257B produced by Kistler Instrument Corporation. As the measured cutting forces are time-dependent and not constant in machining, especially at the moment of cut-in and cut-out, average values of cutting forces measured in the middle stage of the machining process are used in this work.

The workpiece material was 45 % SiCp/Al2024 composites. The average diameter of SiC particles was 5 μm.

**Table 6** Process variables of validation experiments for side grinding force model

| Process variables | Values |
|---|---|
| Spindle speed $n$ (rpm) | 4000, 6000, 8000, 10,000, 12,000, 14,000, 16,000 |
| Feedrate $v_f$ (mm/min) | 200, 300, 400, 500, 600, 700, 800 |
| Cutting depth $a_p$ (mm) | 0.05, 0.1, 0.15, 0.2, 0.25, 0.3, 0.35 |
| Cutting width $b$ (mm) | 1, 1.5, 2, 2.5, 3, 3.5, 4 |

## 4 Results and discussion

### 4.1 Determination of coefficients in the proposed model

#### *4.1.1 Determination of coefficients in side grinding model*

The experimental coefficients $C_1$~$C_7$ could be determined by four groups of experimental data by solving linear equations. To make the model representative for all possible combinations of process parameters which consisted of spindle speed $n$, feedrate $v_f$, cutting depth $a_p$, and cutting width $b$, an orthogonal experiment based on four factors with three levels was conducted, as listed in Table 2.

With the parameter spindle speed large enough, $\frac{2\pi fA}{v_f+v_c}$ is close to 0 (when $n$ is equal to the minimum spindle speed of 8000 rpm with neglected $v_f$, it has the maximum value of 0.0375). So according to Eq. (10), it can be assumed that $l_b = l_a$. For the same reason, it can be assumed that $\cos\varphi = 1$. Hence, the side grinding force model can be simplified as follows:

$$F_{SG} = \begin{cases} C_1\frac{v_f}{nR_o}ba_p + C_3\frac{v_f}{nR_o}\frac{{C_a}^{2/3}}{s^2}b\sqrt{\frac{a_p}{R_o}} + C_6ba_p \\ C_2\frac{v_f}{nR_o}ba_p + C_4\frac{{C_a}^{2/3}}{s^2}b\sqrt{a_pR_o} + C_5\frac{v_f}{nR_o}\frac{{C_a}^{2/3}}{s^2}b\sqrt{\frac{a_p}{R_o}} + C_7ba_p \end{cases} \quad (56)$$

Then each experiment was conducted thrice; the averages of grinding forces were substituted into Eq. (56), and the

**Table 7** Process variables of validation experiments for end grinding force model

| Process variables | Values |
|---|---|
| Spindle speed $n$ (rpm) | 6000, 7500, 9000, 10,500, 12,000, 13,500, 15,000 |
| Feedrate $v_f$ (mm/min) | 50, 100, 150, 200, 250, 300, 350 |
| Cutting depth $a_p$ (mm) | 0.05, 0.1, 0.15, 0.2, 0.25, 0.3, 0.35 |
| Cutting width $b$ (mm) | 6 |

coefficients $C_1$~$C_7$ determined through least square estimation (LSE), as listed in Table 3.

#### *4.1.2 Determination of coefficients in end grinding force model*

An orthogonal experiment based on three factors with four levels was conducted to determine experimental coefficients $C_8$~$C_{11}$, as listed in Table 4.

Then each experiment was conducted thrice; the averages of grinding forces were substituted into Eq. (55), and the coefficients $C_8$~$C_{11}$ determined through LSE, as listed in Table 5.

### 4.2 Predicted influences of process variables on grinding force

The predicted relationships between side grinding force (the normal force and tangential force) and process variables are plotted in Figs. 9 and 10 while the predicted relationships between end grinding force (the axial force) and process variables are plotted in Fig. 11.

Figures 9, 10, and 11 show that all theoretical forces (the normal, tangential, and axial force) nonlinearly decrease with an increase of the spindle speed and approximately linearly increase as the cutting depth and feedrate increase. When the cutting width is increased, the normal force and tangential force also show an approximately linearly increase.

In side grinding process, spindle speed and feedrate have a larger effect on the side grinding force compared with cutting depth and cutting width, especially with the increase of feedrate or decrease of spindle speed, in which both the normal force and tangential force increase obviously.

Figures 9 and 10 also show that the normal force and tangential force vary slightly with the tool parameters (abrasive concentration and size). According to Eq. (41), the tool parameters only have an effect on frictional force which is much lesser than the normal force and tangential force, as shown in Fig. 12. This may be the reason why compared with the process parameters, the tool parameters have a less effect on the side grinding force.

Vibration parameter has the least influence in the side grinding force model. Eqs. (15) and (41) show that only chip formation force in the normal direction is influenced by vibration parameter (vibration amplitude), and as mentioned in Sect. 4.1.1, the excessive spindle speed will weaken the influence of the ultrasonic vibration.

Figure 11 shows that vibration parameters and tool parameters have a larger effect on the end grinding force model

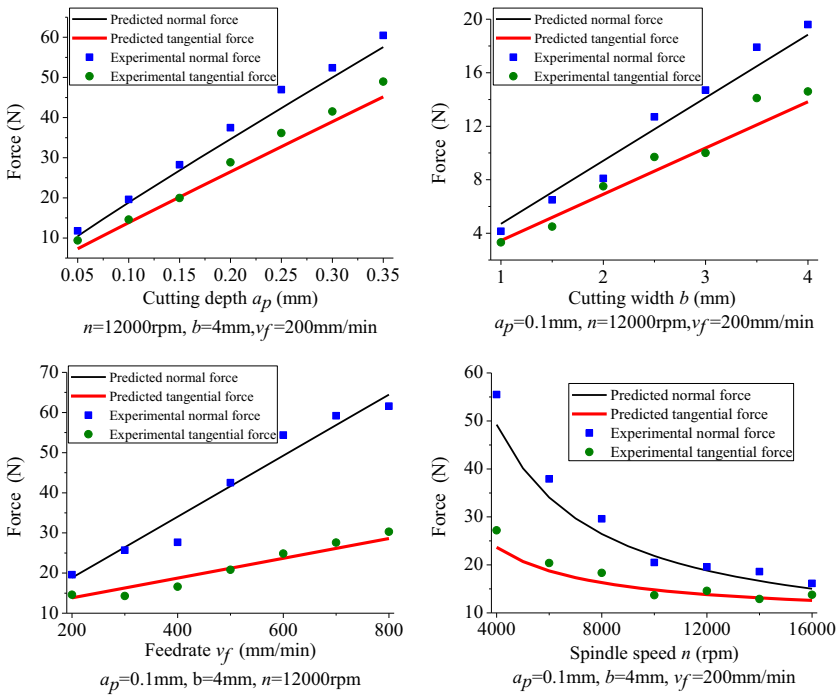


**Fig. 13** Predicted and experimental results of the normal force and tangential force

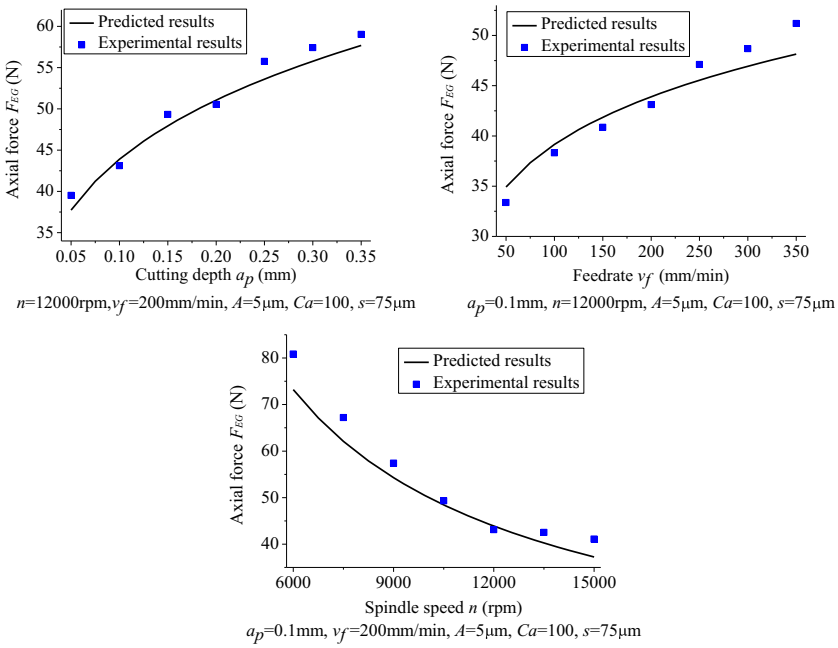


**Fig. 14** Predicted and experimental results of the axial force

compared with the side grinding force model due to the coaxial relations between the vibration direction and the axial force direction. For this reason, vibration parameters and tool parameters have a direct effect on the impact force.

### 4.3 Validation of the proposed grinding force model

The validation experimental setup was the same as shown in Sect. 3, and the process variables for the comparison of predicted values and experimental values of side grinding force model and end grinding force model were listed in Tables 6 and 7, respectively. Each variable was taken in seven levels while keeping other variables constant. Experimental results and predicted results were compared in Figs. 13 and 14.

Figures 13 and 14 showed that the predicted results of the normal force, tangential force, and axial force were found to agree well with the experimental results. It can also be seen that in most cases, the predicted results were smaller than the experimental results. This was due to the fact that in the proposed grinding force model, the ploughing force and erosion force are neglected in side grinding and end grinding, respectively. The average percentage of errors between experimental results and predicted results in the normal force, tangential force, and axial force were 8.6, 11.7, and 5 %, respectively.

## 5 Conclusions

This paper presents a mechanics model for predicting grinding forces in ultrasonic vibration assisted grinding SiCp/Al composites. It consists of side grinding force model and end grinding force model.

In the side grinding force model, the major components are the normal force and tangential force. They can be subdivided into chip formation force, frictional force, and fracture force. In contrast, the axial force developed based on the indentation theory is the major component in end grinding force model.

Based on the proposed model, the relationship between grinding forces and process variables are predicted. The predicted trends show that in side grinding process, both the normal and tangential forces decrease with an increase in the spindle speed and abrasive size and rise with an increase in the cutting depth, cutting width, feedrate, and abrasive concentration. In end grinding process, the axial force increases with a reduction in the spindle speed and abrasive concentration and rises with an increase in the cutting depth, feedrate, vibration amplitude, and abrasive size.

Two groups of single factor experiments were conducted to verify the proposed model, and experimental results are found to agree well with the predicted results. The average percentages of errors between experimental results and predicted results in the normal force, tangential force, and axial force were 8.6, 11.7, and 5 % respectively. Therefore, this model can be used for predicting the grinding forces effectively in ultrasonic vibration assisted grinding of SiCp/Al composites.

**Acknowledgments** This work is supported by the National Natural Science Foundation of China (NSFC) (Grant No. 51375119).

## References


1. Wang Y, Lin B, Zhang XF (2014) Research on the system matching model in ultrasonic vibration-assisted grinding. Int J Adv Manuf Technol 70(1–4):449–458. doi:10.1007/s00170-013-5269-2
2. Shen XH, Zhang JH, Xing DLX, Zhao YF (2012) A study of surface roughness variation in ultrasonic vibration-assisted milling. Int J Adv Manuf Technol 58(5–8):553–561. doi:10.1007/s00170-011-3399-y
3. Bertsche E, Ehmann K, Malukhin K (2012) An analytical model of rotary ultrasonic milling. Int J Adv Manuf Technol 65(9–12):1705–1720. doi:10.1007/s00170-012-4292-z
4. Zhou M, Zhao P (2016) Prediction of critical cutting depth for ductile-brittle transition in ultrasonic vibration assisted grinding of optical glasses. Int J Adv Manuf Technol:1–10. doi:10.1007/s00170-015-8274-9
5. Mahaddalkar PM, Miller MH (2014) Force and thermal effects in vibration-assisted grinding. Int J Adv Manuf Technol 71(5–8):1117–1122. doi:10.1007/s00170-013-5537-1
6. Kishawy HA, Kannan S, Balazinski M (2004) An energy based analytical force model for orthogonal cutting of metal matrix composites. CIRP Ann Manuf Technol 53(1):9–94. doi:10.1016/S0007-8506(07)60652-0
7. Pramanik A, Zhang LC, Arsecularatne JA (2006) Prediction of cutting forces in machining of metal matrix composites. Int J Mach Tool Manuf 46(14):1795–1803. doi:10.1016/j.ijmachtools.2005.11.012
8. Davim JP (2007) Application of Merchant theory in machining particulate metal matrix composites. Mater Des 28(10):2684–2687. doi:10.1016/j.matdes.2006.10.015
9. Dabade UA, Dapkekar D, Joshi SS (2009) Modeling of chip-tool interface friction to predict cutting forces in machining of Al/SiCp composites. Int J Mach Tool Manuf 49(9):690–700. doi:10.1016/j.ijmachtools.2009.03.003
10. Sikder S, Kishawy HA (2012) Analytical model for force prediction when machining metal matrix composite. Int J Mech Sci 59(1):95–103. doi:10.1016/j.ijmecsci.2012.03.010
11. Du JG, Li JG, Yao YX, Hao ZP (2014) Prediction of cutting forces in mill-grinding SiCp/Al composites. Mater Manuf Process 29(3):314–320. doi:10.1080/10426914.2013.864402
12. Ghandehariun A, Hussein HM, Kishawy HA (2015) Machining metal matrix composites: novel analytical force model. Int J Adv Manuf Technol 83(1):233–241. doi:10.1007/s00170-015-7554-8
13. Feng PF, Liang GQ, Zhang JF (2014) Ultrasonic vibration-assisted scratch characteristics of silicon carbide-reinforced aluminum matrix composites. Ceram Int 40(7):10817–10823. doi:10.1016/j.ceramint.2014.03.073
14. El-Gallab M, Sklad M (1998) Machining of Al/SiC particulate metal matrix composites - part II: workpiece surface integrity. J Mater Process Technol 83(1–3):277–285. doi:10.1016/S0924-0136(98)00072-7
15. Tang JY, Du J, Chen YP (2009) Modeling and experimental study of grinding forces in surface grinding. J Mater Process Technol 209(6):2847–2854. doi:10.1016/j.jmatprotec.2008.06.036
16. Patnaik Durgumahanti US, Singh V, Venkateswara Rao P (2010) A new model for grinding force prediction and analysis. Int J Mach Tools Manuf 50(3):231–240. doi:10.1016/j.ijmachtools.2009.12.004
17. Hecker RL, Liang SY, Wu XJ, Xia P, Jin DGW (2007) Grinding force and power modeling based on chip thickness analysis. Int J Adv Manuf Technol 33(5–6):449–459. doi:10.1007/s00170-006-0473-y
18. Agarwal S, Rao PV (2013) Predictive modeling of force and power based on a new analytical undeformed chip thickness model in ceramic grinding. Int J Mach Tool Manuf 65:68–78. doi:10.1016/j.ijmachtools.2012.10.006
19. Tohgo K, Itoh T (2005) Elastic and elastic–plastic singular fields around a crack-tip in particulate-reinforced composites with progressive debonding damage. Int J Solids Struct 42(26):6566–6585. doi:10.1016/j.ijsolstr.2005.04.013
20. Xiao XZ, Zheng K, Liao WH (2014) Theoretical model for cutting force in rotary ultrasonic milling of dental zirconia ceramics. Int J Adv Manuf Technol 75(9–12):1263–1277. doi:10.1007/s00170-014-6216-6
21. Zhang CL, Zhang JF, Feng PF (2013) Mathematical model for cutting force in rotary ultrasonic face milling of brittle materials. Int J Adv Manuf Technol 69(1–4):161–170. doi:10.1007/s00170-013-5004-z
22. Yuan ZW, Li FG, Chen B, Xue FM, Hussain MZ (2014) Further investigation of particle reinforced aluminum matrix composites by indentation experiments. J Mater Res 29(4):586–595. doi:10.1557/jmr.2014.15
23. Yuan ZW, Li FG, Xue FM, Zhang MJ, Li J (2015) An investigation of micro-mechanical properties of Al matrix in SiC/Al composite by indentation experiments. J Mater Eng Perform 24(2):654–663. doi:10.1007/s11665-014-1350-8
24. Yuan ZW, Li FG, Zhang P, Chen B, Xue FM (2014) Mechanical properties study of particles reinforced aluminum matrix composites by micro-indentation experiments. Chin J Aeronaut 27(2):397–406. doi:10.1016/j.cja.2014.02.010